

MODELING CRABBING DYNAMICS IN AN ELECTRON-ION COLLIDER*

A. Castilla^{1,2,3†}, V. S. Morozov², T. Satogata^{1,2}, J. R. Delayen^{1,2}.

¹Center for Accelerator Science, Old Dominion University, Norfolk, VA 23529, USA.

²Thomas Jefferson National Accelerator Facility, Newport News, VA 23606, USA.

³Universidad de Guanajuato (DCI-UG), Departamento de Fisica, Leon, Gto. 37150, Mex.

Abstract

A local crabbing scheme requires $\pi/2 \pmod{\pi}$ horizontal betatron phase advances from an interaction point to the crab cavities on each side of it. However, realistic phase advances generated by sets of quadrupoles or Final Focusing Blocks (FFB), between the crab cavities located in the expanded beam regions and the IP differ slightly from $\pi/2$. To understand the effect of crabbing on the beam dynamics in this case, a simple model of the optics of the Medium Energy Electron-Ion Collider (MEIC), including local crabbing, was developed using linear matrices and studied over multiple turns (1000 passes) of both electron and proton bunches. This model was applied to determine linear-order dynamical effects of the synchro-betatron coupling induced by crabbing.

INTRODUCTION

It is a common practice to use linear models when initially designing and studying machine lattices. Then, special care needs to be taken when looking into non-linear effects in a ring (for example), to avoid higher order resonances that may rise undesirable dynamic conditions for the machine operations (i. e. beam filamentation, beam breakup, etc). Due to the high luminosity requirements imposed on the MEIC [1], stable beam operation while using crossing angle correctors [2] is of a major importance. In the present work we have reduced the entire electron and proton storage rings 6D dynamics to a simple linear map representation [3], excluding the interaction region (IR) (see Fig. 1).

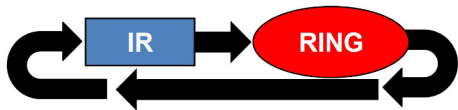


Figure 1: Conceptual sketch of the interaction region (blue) connected on its extremes by a linear map of the ring (red).

Similarly, a simplified model of a symmetric IR using linear elements in the thin lens approximation [4], such as *horizontal crab kickers*, *FFBs*, and *drifts*, was implemented for both electron and proton bunches (see Fig. 2 (a)). A more realistic layout of the current MEIC interaction region is described in Fig. 2 (b). We performed analytical calculations for the propagation of 6D Gaussian bunch distributions

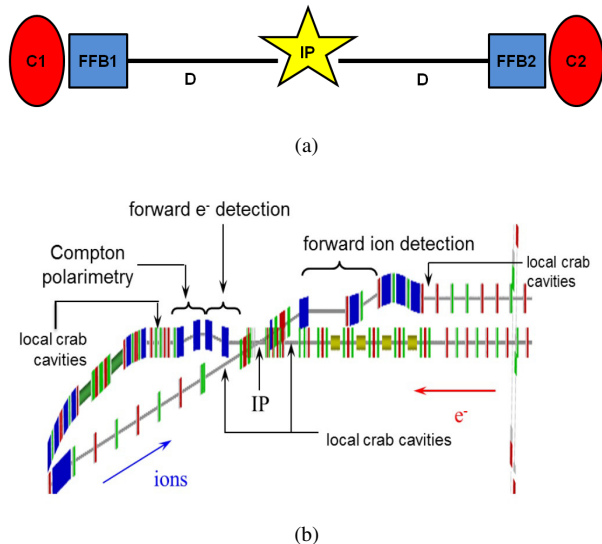


Figure 2: Schematic of the symmetric IR showing the 1st and 2nd crab cavity locations in red (C1 and C2 respectively), the FFBs in blue, the connecting drifts, and the IP in yellow (a). Layout of the current MEIC IR (b).

through the system for a 1000 passes as a first step to study the linear effects on the beams due to implementation of zero-length linear crabbing kicks to account for a 50 mrad total crossing angle. The parameters for the used Gaussian distributions are listed in Table 1.

Table 1: Parameters Used for the Particle's Distributions

Parameter	Electrons	Protons	Units
Energy	5	60	GeV
Number of particles	10^5	10^5	–
$\epsilon_{N,x}$	54	0.35	μm
$\epsilon_{N,y}$	11	0.07	μm
$\sigma_{\Delta p/p}$	7.1	3.0	$\times 10^{-4}$
σ_z	0.75	1	cm

RELATIVE PHASE ADVANCE

The relative phase advance ($\Delta\psi_{x,12}$) constriction for the crab cavities, in a local scheme, states that the bunch should complete an integer number of betatron half oscillations between the crab cavity locations (corresponding to C1 and

* Authored by Jefferson Science Associates, LLC under U.S. DOE Contract No. DE-AC05-06OR23177.

† acastill@jlab.org

C2 for the present work, see Fig. 2) to ensure a complete cancelation of the transverse kick imprinted across the bunch by the crab cavities. Any difference from $n\pi$ in this relative phase advance will cause mismatched conditions on the beams for the ring's optics and will contribute to other effects caused by errors on the crab cavities' voltages, rf phase noise, and particles' time of flight errors, among others.

In the present work we ignored any effects induced by voltage, phase noise, and time of flight errors by using a linear "delta-like" kick at C1 and C2 that would produce the desired crabbed angle at IP, independently of the particles momentum. This linear kick will only account for the individual particle's longitudinal and horizontal positions with respect to the centroid of the bunch. The corresponding transfer matrix is shown in Eqn. 1.

$$M_{\text{Crab}} = \begin{pmatrix} 1 & 0 & 0 & 0 & 0 & 0 \\ 0 & 1 & 0 & 0 & \frac{V_c \tan(\frac{\theta_c}{2})}{D} & 0 \\ 0 & 0 & 1 & 0 & 0 & 0 \\ 0 & 0 & 0 & 1 & 0 & 0 \\ 0 & 0 & 0 & 0 & 1 & 0 \\ \frac{V_c \tan(\frac{\theta_c}{2})}{D} & 0 & 0 & 0 & 0 & 1 \end{pmatrix}, \quad (1)$$

where V_c is the crabbing voltage, θ_c the total crossing angle (50 mrad in this case), and D is the length of the drift placed between the crab cavity location and the IP (see Fig. 2 (a)).

Once the total transfer matrix for the IR is calculated by direct multiplication of all the individual matrices in the proper order, we can compare its m_{12} element (for the horizontal degrees of freedom) to the m_{12} element of the same transfer matrix, but constructed by the standard Courant-Snyder parameterization [4], finding that:

$$\begin{aligned} m_{12} &= 2D \\ &= \sqrt{\beta_x^{C1} \beta_x^{C2}} \sin(\Delta\psi_{x,12}), \end{aligned} \quad (2)$$

where β_x^{C1} and β_x^{C2} are the horizontal β values at the first and second crab cavity locations, respectively, while D refers to the drifts' length as indicated in Fig. 2(a). The only way that this relation accounts for an exact value of $\Delta\psi_{x,12} = n\pi$, is for $\sqrt{\beta_x^{C1} \beta_x^{C2}} \rightarrow \infty$. Therefore, these relative phase advance differences are reduced as the length of the drifts is reduced or the $\sqrt{\beta_x}$ values are increased at the crab cavities' location. Calculations performed, using the lattice design for the MEIC proton storage ring [5], show a relative phase advance difference of $\sim 1\%$ with respect to π .

PROPAGATION OF THE DISTRIBUTIONS

A simple recurrent loop was implemented, using Wolfram Mathematica[®], to propagate the 6D distributions described in Table 1 through the proper matrices' sequence. Special care was taken to store the evolution at several locations within the IP for each turn to account for the evolution of different effects. Figure 3 (a) shows the electron bunch distribution at the IR for the uncrabbed initial distribution (blue), the distribution after 1000 turns without implementing the

crabbing correctors (orange), and finally the bunch after a 1000 turns with local crabbing on (green). Also, Fig. 3 (b) shows the calculated crabbed angle per turn, for the proton bunch with the crabbing correctors turned off (blue) and, when the local crabbing correction is turned on (orange).

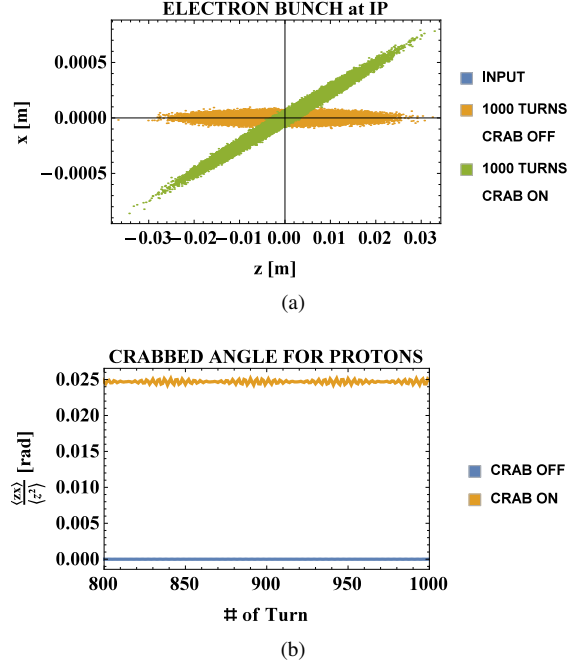


Figure 3: Electron bunch at the IP (a), for the initial condition (blue), after 1000 turns without crabbing (orange), and after 1000 turns with crabbing (green). The calculated proton crabbed angle at IP (b) without crabbing (blue) and with crabbing (orange).

The noticeable periodicity of the effective crabbed angle is consistent with synchrotron and betatron oscillations, induced by a mismatching given by the phase advance differences with respect to π between the crabs. A more detailed analysis of this effect will be presented in the following section of this paper.

Figure 4 (a) shows the electrons distribution at the C1 location, for the initial condition (blue), after 1000 turns with the crabbing correctors off (orange), and after 1000 turns when the crabbing correctors are turned on (green). While, Fig. 4 (b) shows the same for the proton distribution at the C2 location, as a comparison of the similar effects induced by the phase advance differences with respect to π on the bunch orientations for both electrons and protons. These effects do not show indications of resonances that consistently increase the beam sizes, at least at the linear order and for the small number of turns used in this work to track the distributions, but they do produce synchro-betatron coupled oscillations due to the induced beam mismatch.

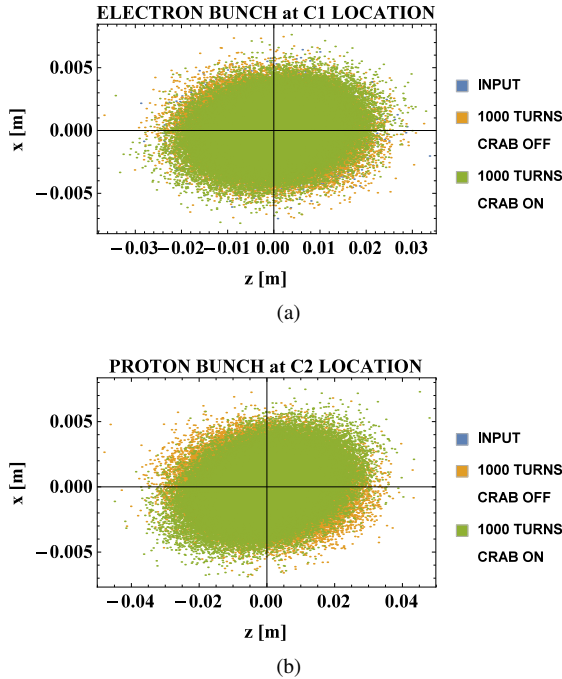


Figure 4: Snapshot of the electron (a) and proton (b) distributions for the initial conditions (blue), after 1000 turns with no crabbing (orange), and after 1000 turns with the crabbing correctors turned on.

SYNCHRO-BETATRON COUPLING

The “snapshots” of the bunch distributions presented above (Fig. 4) show the initial and final conditions after 1000 turns for the mentioned cases. However, we calculated the beamsizes turn by turn at different locations and noticed the correspondent betatron oscillations, when the crabbing correctors are turned off, while for the case, when the crabbing correctors are turned on, synchro-betatron coupling can be observed. The fractional tunes of the whole system are: $\nu_x = 0.73$, $\nu_y = 0.32$, and $\nu_z = 0.01$. A Fourier analysis of the beam size oscillations is presented in Fig. 5 as a function of the tune fraction, since the tunes used in the linear maps for both the electron and proton rings were the same, the Fourier analysis for each case gives the same result with only slight differences in the amplitudes of the peaks, and for this reason we do not distinguish the results for electrons or protons (see Figs. 5 (a) and (b)).

CONCLUSIONS

The analytical linear models for both proton and electron storage rings with simplified symmetric IRs, described in the present work, were used to compare the beam dynamics in an Electron-Ion collider for the cases when perfect crabbing correctors are set to restore geometrical degradation of the luminosity due to a 50 mrad total crossing angle at the IP. We identified an intrinsic difference of the relative horizontal phase advance (from π) between the crab cavities,

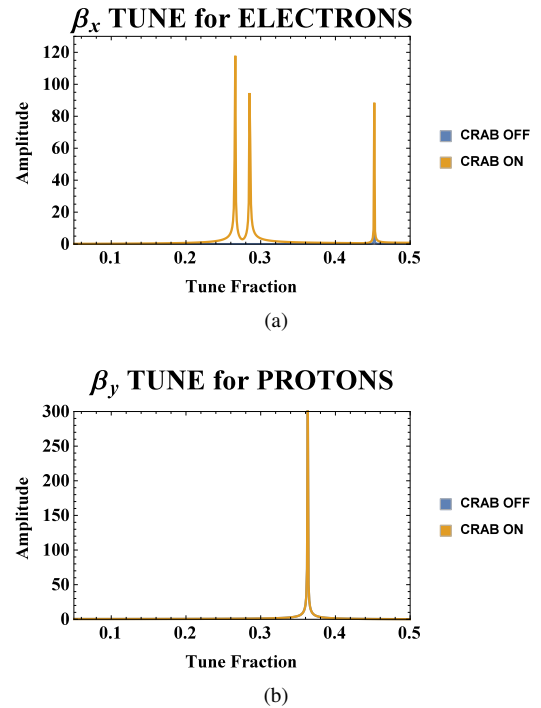


Figure 5: Fourier analysis of the beams’ horizontal (a) and vertical (b) β -functions, for the case when the crabbing correctors are turned off (blue), and when they are turned on (orange).

which depends on the IR’s optics and the physical distance between the crab cavities, for the linear case. Despite this difference being small, it can induce synchro-betatron coupling, showing 2 new sidebands ($\nu_x \pm \nu_z$) in the horizontal betatron motion spectrum. These effects do not give indications of resonances or emittance dilution for the range of turns studied in this work. Further studies of this effects at a linear level for longer number of turns are recommended to ensure stable operation conditions for the beams and to identify possible resonances.

REFERENCES

- [1] S. Abeyratne, et al, “Science Requirements and Conceptual Design for a Polarized Medium Energy Electron-Ion Collider at Jefferson Lab”, JLAB-ACC-12-1619 (2012).
- [2] R. B. Palmer, “Energy Scaling, Crab Crossing and The Pair Problem”, SLAC-PUB 4707 (1988).
- [3] J. Quiang, et al, “Strong-Strong Beam-Beam Simulation Using a Green Function Approach”, PRSTAB 5, 104402 (2002).
- [4] A.W. Chao and M. Tigner, “Handbook of Accelerator Physics and Engineering” 3rd print, World Scientific Publishing Co. (2006).
- [5] A. Castilla, et al, “Effects of Crab Cavities’ Multipole Content in an Electron-Ion Collider”, in Proceedings of IPAC15, Richmond, USA (2015).